THE JOURNAL OF PHYSICAL CHEMISTRY B

Article

Influence of Glass Scaffolds Macroporosity on the Bioactive Process

Joséphine Lacroix,*[,†] Edouard Jallot,[†] Jean-Marie Nedelec,[‡,§] and Jonathan Lao[†]

[†]Clermont University, University Blaise Pascal, CNRS/IN2P3, Particle Physics Laboratory, BP 80026, 63171 Aubière Cedex, France

[‡]Clermont University, ENSCCF, Institute of Chemistry of Clermont-Ferrand, BP 10448, 63000 Clermont-Ferrand, France

[§]CNRS, UMR 6296, ICCF, 63171 Aubière, France

ABSTRACT: Little is known about the ideal morphology for three-dimensional (3D) porous scaffolds to be used in bone tissue engineering. The present study will supply useful data about the dependence of the mineralization process upon macroporous features of bioactive glass scaffolds. It also points out the difficulty in distinguishing between the bioactive properties of scaffolds if using common characterization techniques often considered as standard techniques to assess in vitro bioactivity. Here, two bioactive glass foams with different porosities (porous diameters and interconnection sizes) were successfully synthesized by varying the surfactant quantity in the sol–gel foaming process. The two foams had porosities apparently sufficient to serve as a bone tissue engineering scaffold and exhibited no significant difference when studied for the releasing or the taking up of ionic species when immersed in simulated body fluid (SBF). However, thanks to microion beam analysis, it was possible to highlight key differences in the mineralization reaction taking place at the surface of the pores. It is clearly evident that the homogeneity of reaction inside the 3D-scaffolds is particularly dependent upon porosity. In particular, it is demonstrated that inadequate porous features can result in limited circulation of the fluid inside the pores. Careful attention must be paid to the pore size distribution and interconnection sizes when designing scaffolds for bone tissue engineering, in order to induce homogeneous mineralization inside the porous material and for the scaffold to be efficiently alimented with nutrients or growth factors while allowing a free circulation of the bone cells.

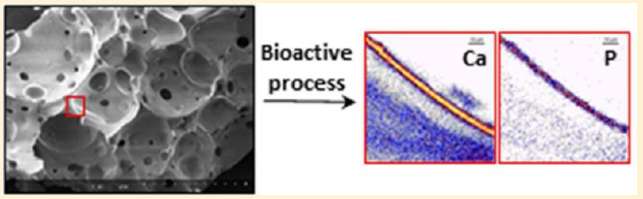

INTRODUCTION

Bone is a fascinating material that can repair itself after a fracture. However, in the case of substantial defects, called "critical defect", for example after a surgical treatment of tumors, bones are unable to regenerate any more.[1] One of the most promising solutions for such a clinical problem is the use of bone tissue engineering. It consists of the artificial fabrication of an implant from cells of the patient grown upon a scaffold with the help of growth factors. The resulting implant would be as efficient as an autologous graft but without the risk of surgical interventions in two different sites and without the limited size of the graft.[2]

A scaffold with specific properties is needed to successfully conduct this cell mediated bone regeneration. A suitable scaffold should be biocompatible, possess a surface allowing cell attachment and proliferation, have an interconnected macroporous structure that enables cell invasion, endure all mechanical solicitation, and be degradable at a rate compatible with the formation of new bone.[3,4] However, bone is a versatile material that exhibits different properties depending on the person and the anatomic site.[5] Consequently, one of the biggest challenges in bone tissue engineering is the design of scaffolds matching the specific features of the targeted site of implantation. In particular, we will see that careful attention must be given to fine control of the porosity.

For bone tissue engineering bioactive glasses are very interesting because of their ability to bond to bone with the formation of a carbonated apatite layer on their surface through the bioactivity process.[6,7] Originally, bioactive glasses were prepared by classic quenching of melts, but the development of sol–gel technology brought new properties to bioactive glasses: a wide variety of compositions can now be obtained and sol–gel derived glasses also own increased specific surface area that improves bioactivity.[8,9] The sol–gel process can furthermore quite easily be adjusted to build materials with specific and tunable properties, e.g., a highly ordered porosity at the nanometer,[10] or even at the micrometer scale. Here we chose the sol–gel foaming process,[11] originally adapted from the in situ polymerization of monomers in a ceramic suspension,[12] to build 3D-highly macroporous materials.

In this work, two sol–gel derived glass foams with significantly different macroporosities were synthesized for use as bone tissue engineering scaffold. To evidence the dependence of the bioactive process upon the foam macroporosity, it is of major importance to study these 3D-porous materials at a local scale during interaction with a biological medium. We will show here how powerful are microion beam analyses (μ-IBA) to achieve this. μ-IBA refers to a set of nuclear-based techniques based on the use of focused ion beams as probes to accurately determine the elemental composition of samples. μ-IBA provides major advantages over more common electron probe microanalysis (EPMA):

Received: October 1, 2012
Revised: December 12, 2012
Published: December 13, 2012

   dx.doi.org/10.1021/jp309731v | J. Phys. Chem. B 2013, 117, 510–517

first, the sensitivity is a hundred times better, due to limited Bremsstrahlung radiation when using heavy charged particles, resulting in a deeply improved signal-to-noise ratio. Second, the spatial resolution can even be better when using a precisely focused ion beam: indeed heavy-charged particles follow a straight path when penetrating the matter, contrary to electrons which associated pear-shaped interaction volume can be very large. Here we used particle induced X-ray emission associated to Rutherford backscattering spectroscopy (PIXE-RBS) to record quantitative elemental maps inside glass foams interacting with biological fluids. It allows monitoring of the physicochemical reactions at the bioactive glass/biological environment interface at a micrometer scale and with an excellent sensitivity (10^{-6} g/g); these are prerequisites for highlighting the influence of the macroporosity onto the biomineralization properties.

EXPERIMENTAL METHODS

Synthesis of Materials. The foaming of a bioactive glass sol has been previously reported by other authors.[13−15] Briefly, a sol of binary glass SiO_2−CaO (75:25 wt %) is made by mixing of TEOS (tetraethylorthosilicate, $Si(OC_2H_5)_4$) with water and hydrochloric acid (2 N). Calcium nitrate ($Ca(NO_3)_2{\cdot}H_2O$) is then added. After 1 h of stirring, a surfactant (teepol) and a catalyst (hydrofluoric acid 5%) are added. Immediately after, the sol is vigorously stirred and poured into cylindrical Teflon containers just before gelation occurs. After 72 h at 60 °C and 48 h at 125 °C, the foams are heated at 700 °C in order to remove the nitrates.[16]

As it was described previously by Jones et al., among all of the parameters implied in the synthesis,[17] the quantity of surfactant has the higher influence on the final porosity.[18] Therefore, the surfactant quantity should be an efficient way to control the scaffold morphology; the two scaffolds tested here were made with different surfactant concentrations (Table 1).

Table 1. Quantities of Reactants Involved in Glass Foams Synthesis

	$H_2O/TEOS_{molar}$	H_2O/HCl_{volume}	V_{HF} (mL)	V_{teepol} (mL)
F1	12	6	0.75	0.25
F2	12	6	0.75	0.5

Characterization of Morphology and Textural Properties. Porosity of the foams was studied by SEM (scanning electron microscopy) observations of scaffolds sections. As it is impossible to know where the sections are realized (following the diameter of a pore or, on the contrary, at the limit of the pore periphery), it is impossible to give an absolute median pore size or interconnection diameter.[19] Indeed, SEM measures of foam sections always minimize the size depending on the cutting plan compared with the diameter of the pore. However, a high number of pictures and measures provide significant and reliable statistics on the apparent pore sizes and interconnection diameters. For that reason at least 50 different diameters were measured for each foam and for each parameter.

Mercury intrusion porosimetry was also used (AutoPore IV 9500, Micromeritics) to compare the two foams.

The mesoporosity of the samples was characterized by nitrogen sorption at 77 K (Quantachrom Autosorb 1). The samples were outgassed under vacuum at 120 °C overnight, the specific surface area determined by the BET (Brunauer Emmet and Teller) method and the mesoporosity studied by the BJH (Barett Joyner and Halenda) method. The total pore volume was obtained for the relative pressure: $P/P_0 = 0.995$.

The total porosities P of the samples are determined by the following formula:

$$P = 100\frac{\rho_{real} - \rho_{app}}{\rho_{real}}$$

ρ_{app} is the apparent density, measured by the ratio between the mass of a scaffold and its volume (geometrically determined). ρ_{real} is the real density of the glass; it has been measured by helium pycnometry and is equal to 2.36 cm^3/g.

In Vitro Assay. To evaluate the bioactivity properties of the foams, they were left to interact with a fluid that mimics ionic plasma composition: SBF (simulated body fluid). During many years, the formation of an apatite layer in SBF was considered as a standard test to evaluate the bioactivity of a material. However recently, some critical issue have been raised from different observations: the pH of the SBF is regulated through a buffer and not through equilibrium with the partial CO_2 pressure as is the case in the body. It does not contain all of the elements of the plasma, like proteins.[20,21] More importantly, there are examples of non in vivo bioactive materials that induce apatite formation in SBF or also bioactive materials that do not induce apatite formation in SBF.[22] Nevertheless, in vitro testing with SBF has often shown a good correlation between the in vivo bioactivity and the apatite formation in vitro and could be considered as an efficient preliminary test for the comparison of materials. The studied composition was also previously tested in contact with bone cells, giving satisfactory results.[23]

The SBF was prepared following recommendations of Bohner et al.[20] A first solution was prepared by the dissolution of NaCl, KCl, $K_2HPO_4{\cdot}3H_2O$, $MgCl_2{\cdot}6H_2O$, Na_2SO_4, and $NaHCO_3$ in deionized water and a second by the dissolution of $CaCl_2$. The pH was buffered with Tris(hydroxymethyl)-aminomethane. The two solutions were filtered and mixed just before interactions in order to obtain clear, sterile, and fresh SBF.

Little pieces of foams were cut and immersed in SBF from 1 h until 10 days, with a constant ratio of 1 mg material per mL of SBF. When the desired time is reached, the pH is measured and the supernatant liquid is filtered and stored for further measurement of ionic composition by inductively coupled plasma atomic emission spectroscopy (ICP-AES). The foam is washed with acetone and dried in order to avoid further reaction. The samples are then embedded in resin (Agar, Essex, England), and sections of 500 μm thickness are cut with a low speed diamond saw.[24] This preparation allows the observation of the bioactive glass/fluid interface but also the analysis of the inner part of the glass.

Microion Beam Analysis. Analyses of the sections were carried out using the nuclear microprobes at the CENBG (Centre d'Etudes Nucléaires de Bordeaux-Gradignan), the AIFIRA Large Scale facility which has been previously described.[25] Measurements permit the identification and the quantification of major and trace elements at the foams/biological fluids interface. PIXE-RBS analysis was performed on the nanobeamline with a proton beam of 3 MeV energy.[26] A proton beam with a diameter nearly 1 μm was used to scan the samples. An 80 mm^2 Si (Li) detector was used for X-ray detection, orientated at 135° with respect to the incident beam axis and equipped with a beryllium window 12 μm thick. The

dx.doi.org/10.1021/jp309731v | J. Phys. Chem. B 2013, 117, 510−517

detector crystal thickness was 4.5 mm, the nominal resolution was 158 eV at the 5.9 keV Mn Kα line. The software SUPAVISIO was used to define the different regions of interest with the use of masks. These masks isolate the spectra corresponding to the region of interest in order to calculate the elemental composition in that region. Quantification is done thanks to the use of the software GUPIX and is calibrated against NIST standard reference glass materials.

RESULTS

Morphological and Textural Properties. No significant difference was observed between the two foams in term of texture (Table 2). Indeed, the specific surface area, total pore volume, and average pore diameter are similar. The total porosities are respectively 83 ± 4% and 88 ± 2% for F1 and F2, meaning both foams are highly porous without significant difference. They both exhibit high porosity and high surface area that would improve bioactivity.

Table 2. Mesoporosity of the Foams Studied by Nitrogen Sorption

	F1	F2
total pore volume (cm^3/g)	0.50 ± 0.05	0.50 ± 0.03
average pore diameter (nm)	6.3 ± 0.2	6.7 ± 0.3
specific surface area (m^2/g)	158 ± 12	152 ± 16

However, a difference in macroporosity is observed by mercury intrusion porosimetry with measured pores between 20 and 175 μm and an average pore diameter of 34 μm for F1 and pores between 10 and 300 μm and an average pore diameter of 123 μm for F2. Nevertheless, the values obtained by mercury intrusion are very low compared to the high number of pores above 200 μm that are directly observed on SEM pictures. Mercury intrusion porosimetry is a widely used technique for the study of porous materials, but this technique is limited to the pores smaller than 250 μm.[18] As a consequence, it does not allow one to study the complete macropore size distribution. On the contrary, measurements on SEM pictures (Figure 1) allow the direct observation of pore size and interconnection distributions (Figures 2 and 3) even with the biggest pores. For F1, 89% of pore diameters are between 100 and 300 μm and 76% of interconnections are under 100 μm. For F2, 64% of pores have diameters higher than 300 μm and 53% of interconnections are between 100 and 300 μm.

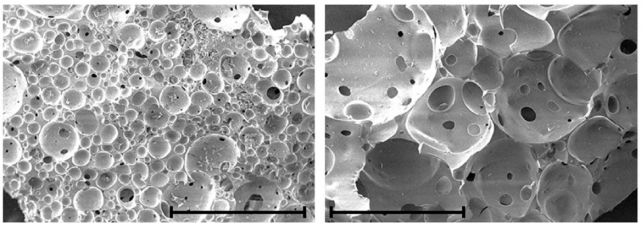

Figure 1. SEM pictures (scale bar: 1 mm) of foams F1 (left) and F2 (right).

Variations of SBF ionic composition and pH values. When immersed in SBF, all foams lead to a similar evolution for SBF ionic composition, regardless of their porous characteristics (Figure 4). Before 1 day of immersion, silicon and calcium concentrations increase rapidly in the biological medium. After 1 day of immersion, their concentrations reach a maximum of 55 and 260 $\mu g \cdot g^{-1}$ respectively for Si and Ca. Concerning phosphorus and magnesium concentrations, they decrease with time of interaction with SBF and after 5 days they reach a minimum of 0 and 53 $\mu g \cdot g^{-1}$, respectively. Evolutions of pH in SBF are similar for the two foams. Before 1 day, the pH increases from 7.40 to 7.57 and 7.61 respectively for foams F1 and F2. After 2 days, the pH stays constant in the biological medium.

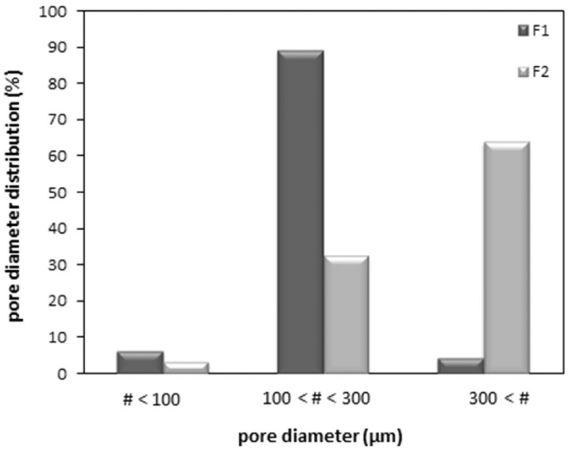

Figure 2. Pore size distribution (%).

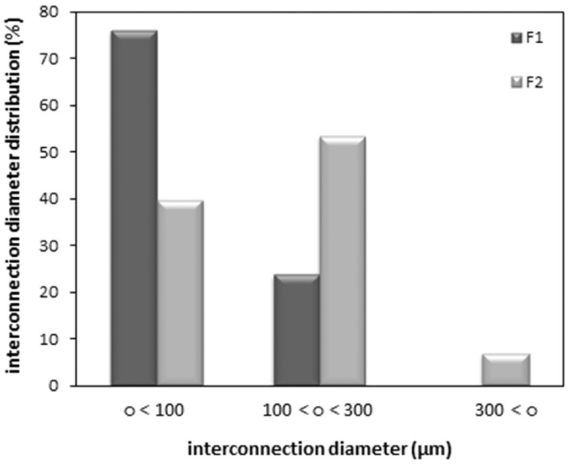

Figure 3. Interconnection size distribution (%).

Elemental Mapping at the Fluid/Bioactive Foam Interface. At each position of the microbeam on the sample, X-rays are detected, and by a scanning of a defined region it is possible to realize elemental mapping (Figures 5−7). The concentration of an element increases with respect to the color scale. This means that the white regions do not contain the mapped element. Silicon and calcium maps at 0 day confirmed the homogeneity of the binary glass (Figure 5). On the calcium map, the central pore seems to contain calcium. It is an experimental artifact that appears because the thickness of the sections cut is in the same magnitude as the pore diameter. Assume the pores to be spherical: if the cutting does not pass through the center of the pores, then the portions of spheres cut may appear as spherical caps rather than annular rings. As a consequence the spherical cap (i.e., upper or lower portion of a pore) will be evidenced by the presence of material under the surface of the section. In this condition it is possible to detect the heavier elements (because of the higher energy of the

dx.doi.org/10.1021/jp309731v | J. Phys. Chem. B 2013, 117, 510−517

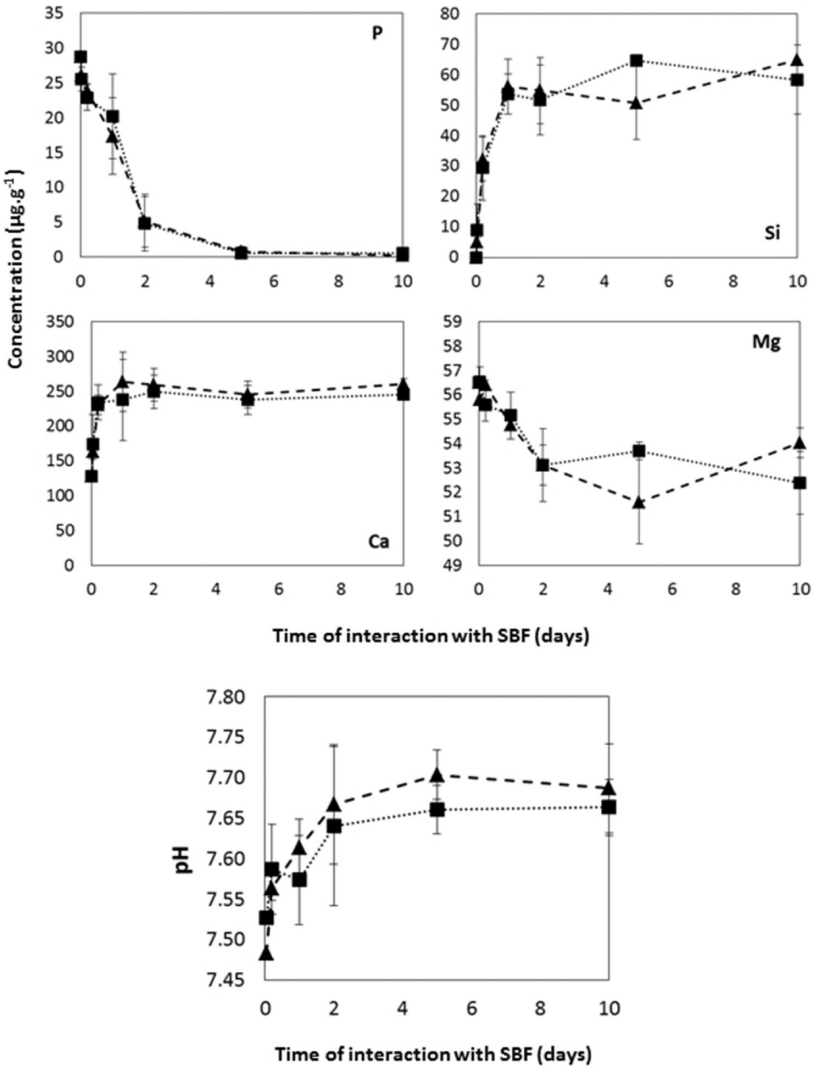

Figure 4. Variations of the ionic composition and pH value of the biological fluid during immersion of the two foams F1(■) and F2 (▲) in SBF.

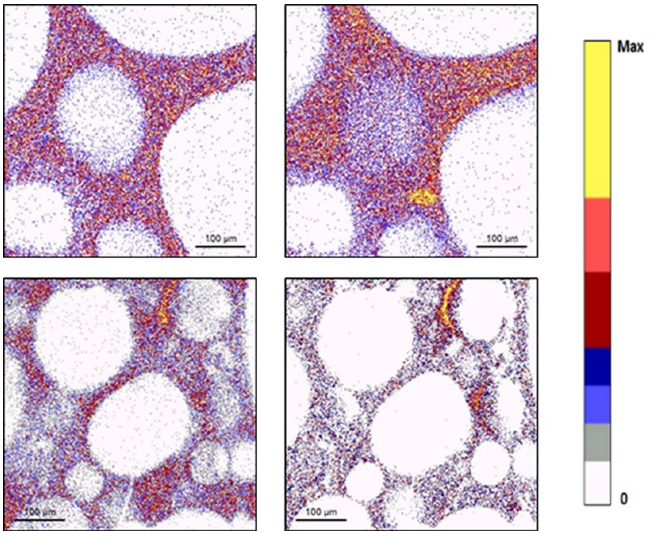

Figure 5. Chemical mapping (from left to right: silicon and calcium) of F1 (top) and F2 (bottom) before interaction with SBF (maps of 500 μm × 500 μm).

corresponding X-rays) coming from the deep regions of the section, like here for calcium in Figure 5.

From silicon, calcium, and phosphorus maps at 10 days of interaction (Figure 6) we can deduce two very different bioactive behaviors depending on the porous characteristics of the foams. The bioactive mechanism was expected to lead to an homogeneous mineralization process at the surface of the pores throughout the material. It is the case for F2, with the formation of a CaP layer of approximately 5 μm in thickness that can be seen after 5 days of interaction in Figure 7. For F1, the mineralization process rather consists of a bulk reaction beginning in the outer part of the foam, i.e. in the peripheral regions "directly" exposed to the fluids. For F1 large areas are mineralized but not throughout the scaffold, the core regions being not really affected. For F2 the mineralization process is "diluted" as it induces a homogeneous deposition of calcium and phosphorus throughout the scaffold.

Evolution of the Local Concentrations. Two distinct kinds of regions were studied: the inner parts of the walls (that were initially not in direct contact with the fluid) which were left unreacted regarding mineralization, and the mineralized surfaces of the walls which are entirely changed into a CaP layer at the later stages.

dx.doi.org/10.1021/jp309731v | J. Phys. Chem. B 2013, 117, 510−517

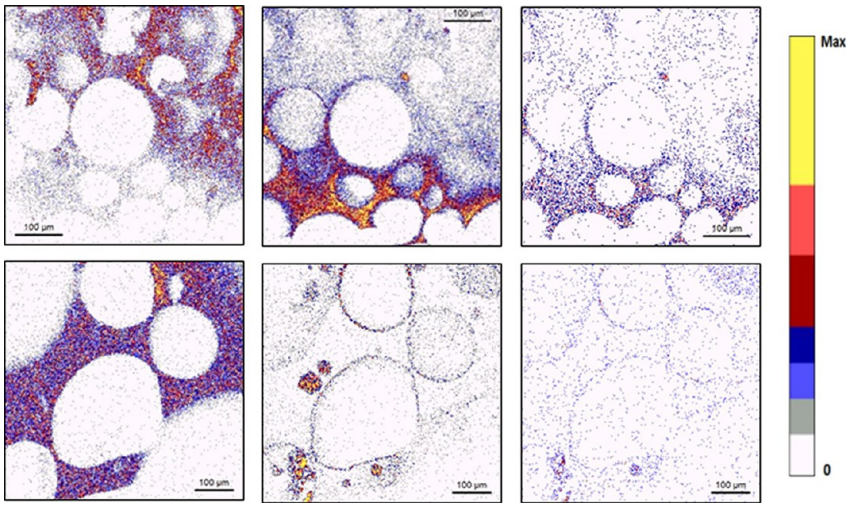

Figure 6. Chemical maps (from left to right: silicon, calcium, and phosphorus) for the two foams at 10 days of interaction with SBF (maps of 500 μm × 500 μm for F1 and 600 μm × 600 μm for F2).

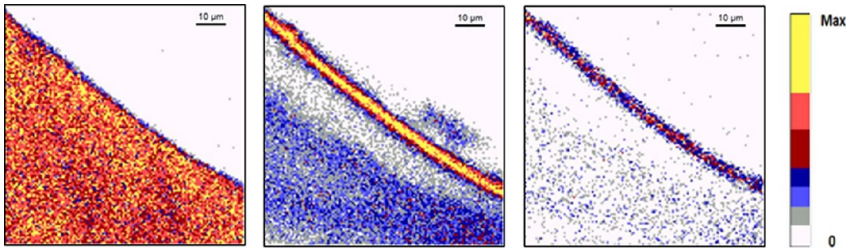

Figure 7. Chemical maps (from left to right: silicon, calcium, and phosphorus) at the pore surface of F2 foam at 5 days of interaction with SBF (maps of 80 μm × 80 μm) .

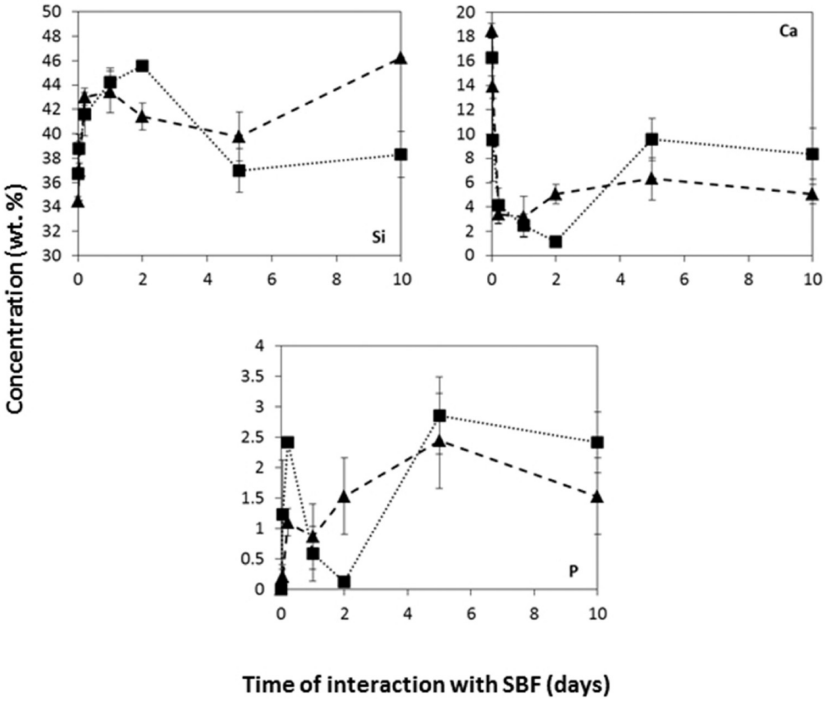

Figure 8. Variation of the local concentrations in the inner part of the walls for F1 (■) and F2 (▲) during immersion in SBF.

The evolution of the concentration in the inner part of the walls (Figure 8) shows a rapid decrease of the calcium content in the earlier stage of reaction. At the same time an increase in Si is logically observed, Si and Ca concentrations being closely tight together. After 2 days, Ca concentration increases between 5 and 10 wt % whereas Si concentration decreases. At the same

dx.doi.org/10.1021/jp309731v | J. Phys. Chem. B 2013, 117, 510−517

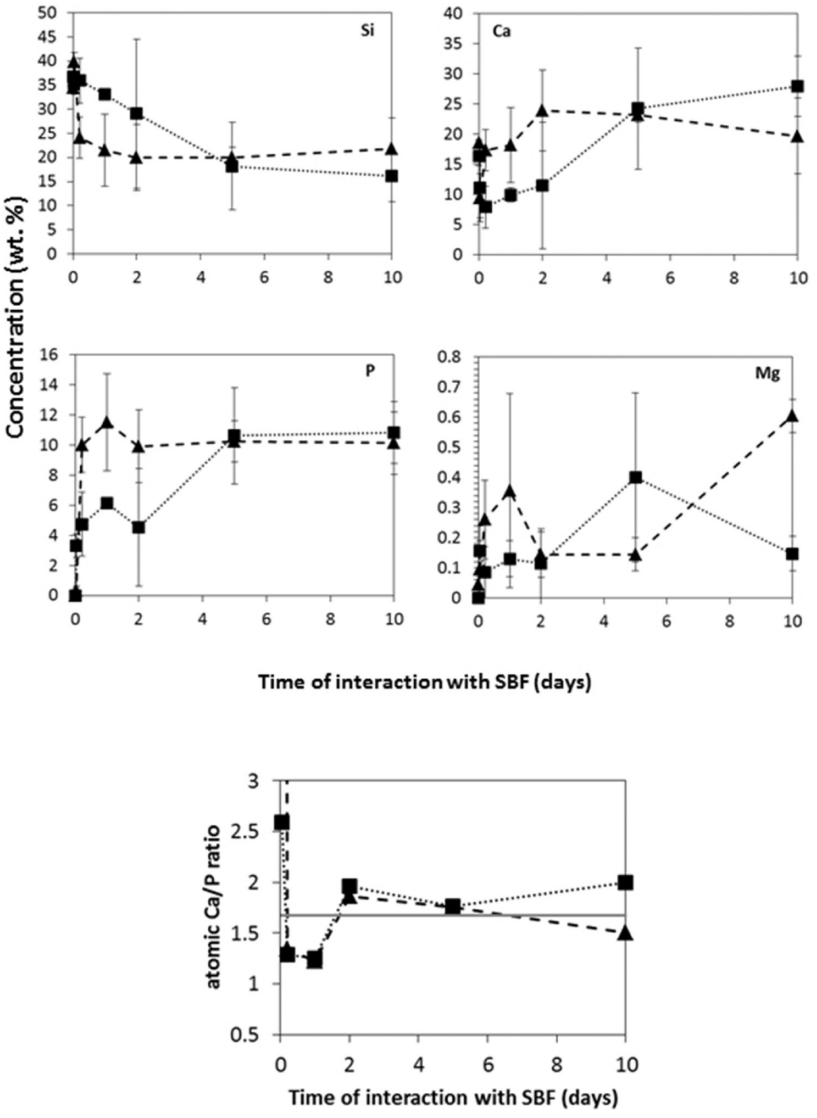

Figure 9. Variation of the local concentrations and atomic Ca/P ratio at the surface of the walls for F1 (■) and F2 (▲) during immersion in SBF (blue line; HA, hydroxyapatite).

time, phosphorus coming from the fluids is detected in the inner part of the walls at a concentration approximately of 2 wt % showing evidence of a diffusion process.

The inner composition of the walls was determined accurately, the measurements being well reproducible. This is not the case with the mineralized surface layer, and its average composition is associated with high uncertainties (Figure 9). This phenomenon is not due to the measurement technique itself, which presents a very high sensitivity, but it comes from discrepancies in the mineralization process. Indeed, even for F2 that involves the homogeneous deposition of calcium phosphates, significant disparities are observed in the composition of the newly formed surface layer. It is not that surprising as it is well-known that the mineralization process involves the formation of metastable phases to bone-like apatite.[27] Concentration values given in Figure 9 are an average of three measurements for each foam. Higher uncertainties are calculated for F1 because of its higher inhomogeneity toward mineralization. It is worth noting that for both kinds of foams the uncertainties decrease with time of interaction with SBF: this is well correlated to the gradual transformation of the Ca−P transient phases into more stable biological apatite as the mineralization further progresses. In the two foams, the Mg content increases at the periphery of the glass which is in agreement with the observed decrease of Mg in the SBF. Mg is incorporated as a trace element in the CaP layer, especially for F1 where it reaches the value of 0.6 wt %. The evolution of the molar Ca/P ratio (Figure 9) in the mineralization layers of the two foams shows that after a few days of interaction it is close to the 1.67 ratio of stoichiometric hydroxyapatite.

■ DISCUSSION

Porosity analysis demonstrated that the foams made with less surfactant (F1) exhibit smaller pore diameters and smaller interconnections than the foams made with more surfactant (F2). Adjusting the quantities of surfactant is an efficient way of controlling pore diameters and interconnections. As can be seen in Figure 2, both F1 and F2 foams have pore diameters larger than 100 μm and are interconnected. It is often argued, without a real demonstration, that scaffolds owning such morphologies could be interesting candidates for bone tissue engineering.[28] This seems to be confirmed when using another

dx.doi.org/10.1021/jp309731v | J. Phys. Chem. B 2013, 117, 510−517

routine test commonly used to evaluate the bioactivity: the ICP-AES characterization of SBF. With regard to the evolution of concentrations in SBF, the two foams are equivalent. The observed trends are consistent with what is known about the bioactive mechanism, which involves (1) the rapid dealkalization of the glass through exchanges with protons from the biological solution, leading to an increase in Ca^{2+} in SBF and a subsequent pH increase, (2) the breakup of the silicate network associated to the release of silicic acid in SBF, and (3) the mineralization of a calcium phosphate layer at the bioactive glasses surface involving the taking up of Ca and P from SBF.

We have seen that significant differences can be highlighted with μ-IBA (PIXE-RBS) quantitative imaging of the scaffolds. From Figure 9 it is visible that during the early stages of the bioactive process, increased kinetics of reaction is observed in the mineralized layer for F2; in fact for F2 the Si content decreases more quickly, whereas the increase in Ca and P is faster.

To better understand the origin of such different behaviors for F1 and F2 foams, two tests of fluid penetration were carried out. In the first one the foams were immersed in SBF mixed with black ink during 5 min: it clearly showed that the fluid easily penetrated throughout the scaffolds for F1 and for F2, as the initially white foams became totally tainted in black after immersion. This means that all areas inside the scaffold were allowed to be in contact with the fluid.

A second test was carried out by immersing the two foams in SBF first mixed with pale blue ink, and after 5 min, black ink was added. The foams were then agitated for 3 h before being removed from the fluid, dried, and cut. Figure 10 shows optical

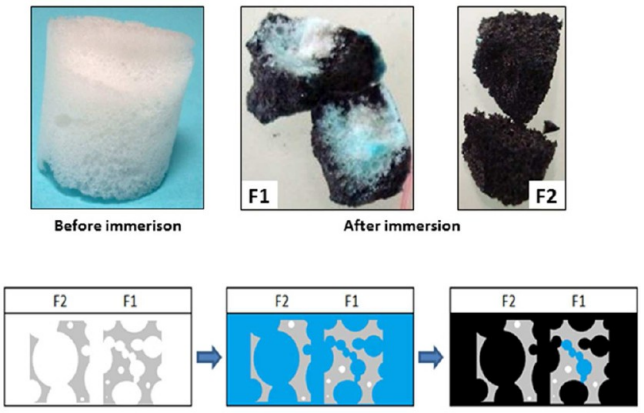

Figure 10. Optical micrographs of the sections of foams (F1 and F2) after immersion in SBF tainted with ink and schematic description of the test. The two foams are immersed in SBF tainted with blue ink, after 5 min black ink is added and colors the interior of F2 through fluid circulation but is unable to color F1 because of fluid confinment.

micrographs of the results: for F1 the inner parts (core regions) of the foam remained essentially blue. On the contrary, F2 was entirely tainted in black. This suggests that the macroporosity inside F1 is insufficient to allow a real circulation of the fluid inside the scaffold. In F1 the fluid penetrates by capillary action as proven by the first test, but remains then confined into the pores or slowly renewed. Indeed the behavior of fluids circulating inside channels less than 1 mm is dominated by parameters like surface tension, capillarity and fluidic resistance, because as dimensions shrink the relative importance of surface to volume forces increases .[29] For F2 the pore diameters and interconnection sizes are both larger, the circulation of fluids is easier and μ-PIXE analysis has shown that it will result in homogeneous mineralization reactions throughout the scaffolds. F1, when in contact with cells would result in poorly fed material due to poor circulation of fluids. Moreover, the poor mineralization evidenced by μ-PIXE would limit cell attachment inside the scaffold and so the colonization by cells.

As the problem of fluid circulation is of major concern in vivo, further studies on implanted foams are planned.

CONCLUSION

Little is known about the ideal specific morphology for 3D-porous scaffolds to be used in bone tissue engineering. Our study highlighted the influence of the pore diameter distributions and interconnection sizes onto the mineralization process inside promising candidates for bone tissue engineering, namely bioactive glass scaffolds. The synthesis of scaffolds with different porosities was possible thanks to efficient variations in operating conditions during the sol−gel foaming process. Commonly used techniques were unable to differentiate the bioactive properties of the scaffolds, from which it could be erroneously concluded that both are suitable for bone tissue engineering. Hopefully the use of microion beam analysis evidenced two different mineralization behaviors depending on the scaffold morphology: one is associated with a porous structure that would confine the biological fluids when immersed whereas the second one allows the free circulation of the fluids.

It points out that suitable morphologies for bone tissue engineering scaffolds cannot be defined by the classic criteria of pores of a few hundred micrometers with interconnections. It rather seems that a minimum interconnection size or number is necessary to allow an easy circulation of fluids, not only for cells to be easily alimented with nutrients and growth factors but also because it would result into a poor mineralization of the inner surface of the scaffold.

AUTHOR INFORMATION

Corresponding Author

*E-mail: josephine.lacroix@clermont.in2p3.fr. Tel: +33(0) 4 73 40 72 71. Fax: +33(0) 4 73 26 45 98.

Notes

The authors declare no competing financial interest.

ACKNOWLEDGMENTS

This work was supported by ANR in the National Program "Blanc" BLAN (Projet "NANOSHAP" ANR-09-BLAN-0120) and was granted by the Conseil Régional d'Auvergne.

REFERENCES

(1) Schroeder, J. E.; Mosheiff, R. *Injury* **2011**, *42*, 609−613.
(2) Blitch, E. L.; Ricotta, P. J. *J. Foot Ankle Surg.* **1996**, *35*, 458−462.
(3) Jones, J. R. *J. Eur. Ceram. Soc.* **2009**, *29*, 1275−1281.
(4) Pena, J.; Roman, J.; Cabanas, M. V.; Vallet-Regi, M. *Acta Biomater.* **2010**, *6*, 1288−1296.
(5) Fu, Q.; Saiz, E.; Rahaman, M. N.; Tomsia, A. P. *Mater. Sci. Eng., C* **2011**, *31*, 1245−1256.
(6) Hench, L. L.; Wheeler, D. L.; Greenspan, D. C. *J. Sol-Gel. Sci. Technnol.* **1998**, *13*, 245−250.
(7) Jones, J. R.; Sepulveda, P.; Hench, L. L. J. *Biomed. Mater. Res.* **2001**, *58*, 720−726.
(8) Arcos, D.; Vallet-Regi, M. *Acta Biomater.* **2010**, *6*, 2874−2888.

(9) Saravanapavan, P.; Jones, J. R.; Pryce, R. S.; Hench, L. L. *J. Biomed. Mater. Res. A* **2002**, *66*, 110−119.
(10) Wu, C.; Fan, W.; Gelinsky, M.; Xia, Y.; Simon, P.; Sculze, R.; Doert, T.; Luo, Y.; Cuniberti, G. *Acta Biomater.* **2011**, *7*, 1797−1806.
(11) Sepulveda, P.; Jones, J. R.; Hench, L. L. *J. Biomed. Mater. Res.* **2002**, *59*, 340−348.
(12) Sepulveda, P.; Binner, J. G. P. *J. Eur. Ceram. Soc.* **1999**, *19*, 2059−2066.
(13) Jones, J. R.; Lee, P. D.; Hench, L. L. *Philos. Trans. R. Soc. A* **2006**, *364*, 263−281.
(14) Jones, J. R.; Sepulveda, P.; Hench, L. L. *Key. Eng. Mater.* **2002**, *218−220*, 299−302.
(15) Valerio, P.; Guimaraes, M. H. R.; Pereira, M. M.; Leite, M. F.; Goes, A. M. *J. Mater. Sci.: Mater. Med.* **2005**, *16*, 851−856.
(16) Lin, S.; Ionescu, C.; Pike, K. J.; Smith, M. E.; Jones, J. R. *J. Mater. Chem.* **2009**, *19*, 1276−1282.
(17) Jones, J. R.; Hench, L. L. *J. Biomed. Mater. Res. B* **2004**, *68*, 36−44.
(18) Jones, J. R.; Hench, L. L. *J. Mater. Sci.* **2003**, *38*, 3783−3790.
(19) Jones, J. R.; Lin, S.; Yue, S.; Lee, P. D.; Hanna, J. V.; Smith, M. E.; Newport, R. J. P. I. *Mech. Eng. H* **2010**, *224*, 1373−1387.
(20) Bohner, M.; Lemaitre, J. *Biomaterials* **2009**, *30*, 2175−2179.
(21) Pan, H.; Zhao, X.; Darvell, B. W.; Lu, W. W. *Acta Biomater.* **2010**, *6*, 4181−4188.
(22) Kokubo, T.; Takadama, H. *Biomaterials* **2006**, *27*, 2907−2915.
(23) Isaac, J.; Nohra, J.; Lao, J.; Jallot, E.; Nedelec, J. M.; Berdal, A.; Sautier, J. M. *Eur. Cells Mater.* **2011**, *21*, 130−143.
(24) Jallot, E.; Lao, J.; John, L.; Soulié, J.; Moretto, P.; Nedelec, J. M. *Appl. Mater. Interfaces* **2010**, *2*, 1737−1742.
(25) Incerti, S.; Zhang, Q.; Andersson, F.; Moretto, P.; Grime, G. W.; Merchant, M. J.; Nguyen, D. T.; Habchi, C.; Pouthier, T.; Seznec, H. *Nucl. Instrum. Methods B* **2007**, *260*, 20−27.
(26) Barberet, P.; Daudin, L.; Gordillo, N.; Sorieul, S.; Simon, M.; Seznec, H.; Idarraga, I.; Incerti, S.; Balana, A.; Moretto, P. *Nucl. Instrum. Methods B* **2011**, *269*, 2163−2167.
(27) Dorozhkin, S. V.; Epple, M. *Angew. Chem., Int. Ed.* **2002**, *41*, 3130−3146.
(28) Karageorgiou, V.; Kaplan, D. *Biomaterials* **2005**, *26*, 5474−5491.
(29) Stone, H. A.; Stroock, A. D.; Ajdari, A. *Annu. Rev. Fluid Mech.* **2004**, *36*, 381−411.